Article

NOx Abatement by a TiO$_2$-Based Coating under Real-Life Conditions and Laboratory-Scale Durability Assessment

Julie Hot [1,*], Clément Fériot [1], Emilie Lenard [1] and Erick Ringot [1,2]

[1] Laboratoire Matériaux et Durabilité des Constructions (LMDC), INSA/UPS Génie Civil, 135 Avenue de Rangueil, CEDEX 4, 31077 Toulouse, France; clement.feriot@laposte.net (C.F.); emilie.lenard@gmail.com (E.L.); ringot@lrvision.fr (E.R.)
[2] LRVision SAS, 695 Rue de l'Hers, Zone d'Activité de la Masquère, 31750 Escalquens, France
[*] Correspondence: hot@insa-toulouse.fr

Abstract: In urban environments, various pollutants generated by road traffic, human, and industrial activities degrade outdoor and indoor air quality. Among these pollutants, nitrogen oxides (NOx) are subject to air quality regulations designed to protect human health and the environment. It is therefore crucial to keep their concentration as low as possible. Advanced oxidation processes are a practical choice for the degradation of NOx; among them, heterogeneous photocatalysis has proven to be a viable route. However, while the efficiency of this process has been widely demonstrated on a laboratory scale, it is still the subject of debate for real-life applications. The purpose of this study was to present a new field experiment on the application of a photocatalytic coating to outdoor walls. Air quality monitoring stations were used to evaluate the NOx concentration reduction instead of the chemiluminescent analyzer, in order to increase the number of sampling points. Statistical analysis was carried out to interpret the results. Density probability functions were plotted and showed a positive impact of the coating, leading to lower NOx concentrations. This work was completed by a laboratory-scale assessment of the coating's durability using abrasion, QUV, and immersion/drying tests. The air depollution capacity of the chosen coating was significantly reduced after QUV testing.

Keywords: air quality; NOx depollution; photocatalysis; TiO$_2$-based coating; field conditions; low-cost sensors; durability

1. Introduction

The deterioration of outdoor air quality has become a major global concern, both in terms of human health and the economic costs of healthcare. According to the World Health Organization (WHO), nine out of ten people breathe air containing high levels of pollutants, and outdoor and indoor air pollution causes 7 million premature deaths every year [1]. Among atmospheric pollutants, nitrogen oxides (NOx) play a predominant role and have proven harmful effects on health. In particular, nitrogen dioxide (NO$_2$) is known to cause diabetes mellitus, respiratory problems (asthma), cardiovascular disease (stroke), and other adverse effects on the immune system [2–5]. NO$_2$ is also a potential carcinogen [6,7]. NOx are emitted during all combustion processes using fossil fuels, such as heating, electricity generation, and the transport industry (the road transport sector was the main source of reported NOx emissions, responsible for 41%, followed by the energy supply sector with 17% of emissions in the EU Member States in 2021) [8–12]. Urban areas are particularly affected by air pollution, with road traffic being one of the main sources of NOx, emitted principally in the form of NO [13,14]. NO$_2$ is a secondary pollutant formed mainly by a photolysis reaction between NO and O$_3$ [15,16]. From an environmental point of view, NO$_2$, along with sulfur dioxide (SO$_2$), is also involved in the formation of acid rain, reacting with water to form nitric and nitrous acids, leading to degradation of human patrimony and deterioration of soil and freshwater ecosystems due to the modification of

their chemical composition [17]. Moreover, NOx coming mainly from outside can infiltrate buildings and affect indoor air quality.

In 2021, the WHO revised the NO_2 threshold limits and recommended that a value of 10 $\mu g \cdot m^{-3}$ annual average or 25 $\mu g \cdot m^{-3}$ 24-h average should not be exceeded (instead of the previous values of 40 $\mu g \cdot m^{-3}$ annual average and 200 $\mu g \cdot m^{-3}$ 1-h average) [18]. However, this new annual average guideline is far from being met in 2021 in European countries, as shown in Figure 1, and 52,000 deaths were attributable to the exposure to NO_2 concentrations above the WHO air quality guideline level of 10 $\mu g \cdot m^{-3}$ in the EU-27 (Member States) [5]. To help cope with this burden, air quality plans are defined to improve air quality, reduce air pollutant emissions, and bring benefits to public health. Air quality plan policy focuses mainly on traffic planning and management (improving public transport, management of parking spaces, speed limits, low-emission zones, and modal shifts in transport), public information and education through different media channels, and the use of low-emission fuels [19].
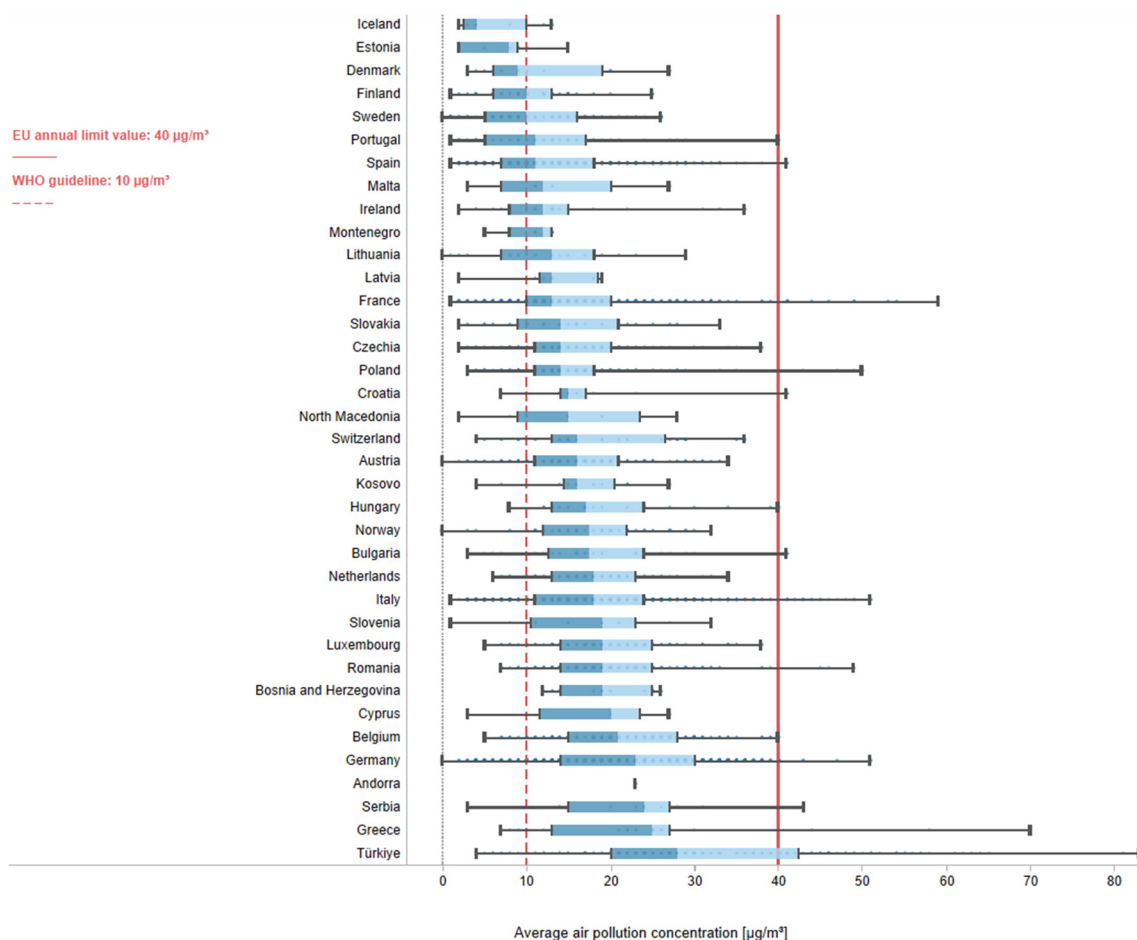
Figure 1. NO_2 average concentration in 2021 in $\mu g \cdot m^{-3}$ and in relation to the EU annual limit value and the WHO annual guideline value. Per country, the minimum and maximum concentrations, the median, and the percentiles 25 ("Lower Hinge") and 75 ("Upper Hinge") of all the measurements are shown via boxplots [20].

In France, almost 80% of the population lives in urban areas and is therefore exposed to heavy road traffic, domestic heating, and local industry. To optimize urban space and increase population density, the layout of buildings tends to form narrow corridors where air pollution accumulates. Exploiting the surfaces of existing or new buildings to capture gaseous pollutants appears to be an interesting way to decrease their concentration and,

therefore, improve outdoor and indoor air quality. This can be done using catalytic [21–23] or photocatalytic [24–26] processes, which are promising technologies for NOx degradation.

The photocatalysis technique, which requires just three components—a semiconductor (catalyst), an emitted photon (sunlight or artificial light), and a powerful oxidizing agent (oxygen, moisture)—is based on the generation of reactive oxygen species and water vapor, which have the potential to mineralize a wide range of pollutants through redox reactions under ambient conditions. Various photocatalysts and modification strategies have been studied for NO removal, with the main aim of improving its conversion and reaction selectivity [27,28]. Among them, titanium dioxide (TiO_2) has attracted great interest in heterogeneous photochemistry [29] and is the reference photocatalyst for air purification due to its high oxidation capacity, stability, availability, and low cost [30,31]. Cement manufacturers offer products incorporating this semiconductor in bulk as an additive. A number of studies in the literature focus on the air depollution property of cementitious materials with added TiO_2 [32,33]. At the concrete scale, however, particles of the semiconductor are lost in the internal structure because they are inaccessible to light and gaseous pollutants present in the air. Moreover, this technique is not possible for other materials with specific manufacturing processes, such as brick or wood. Surface application via a coating offers the advantage, on the one hand, of treating existing structures and, on the other, of optimizing the quantity of the semiconductor required at the air/material interface, thus reducing costs [34].

Numerous articles demonstrate the effectiveness of photocatalytic coatings in reducing NOx concentration under laboratory conditions [25,35], approximating those found indoors [36,37], or by model simulation [38,39]. For most of them, experimental parameters (relative humidity, radiation, initial NOx concentration, etc.) are often adjusted to optimize photocatalysis efficiency. These parameters can be easily managed on a laboratory scale, unlike in real conditions, meaning that the effectiveness of NOx reduction using a TiO_2-based coating may be lower in a real environment than in laboratory experiments. Fewer articles deal with the photocatalytic degradation of NOx in real-world conditions, and results showed variability in performance depending on the environmental conditions. Maggos et al. observed that the effectiveness of a TiO_2-based photocatalytic coating applied to walls varied from 36.7 to 82% [40]. In particular, the authors showed that wall orientation, wind direction, and solar irradiance were the main factors behind this variation in efficiency. Folli et al. observed a reduction in NOx degradation with relative humidity and an increase with temperature; an average of 22% NOx degradation and a maximum of 45% were obtained with concrete paving stones containing TiO_2 [41]. More recently, Brattich et al. observed a reduction in NOx of between 14 and 21% in both real and simulated conditions [42]. Further references on real-life experiments can be found in a review by Russel et al. [43]. The photocatalytic process also raises the question of long-term durability and efficiency. These aspects, along with the efficiency assessment under field conditions, are of the utmost importance in demonstrating the technology readiness level of such a process. Further studies are still needed in these areas.

The present article focuses on two practical aspects of NOx photocatalytic depollution. It proposes to report a new field test to evaluate the performance of a photocatalytic coating to reduce NOx concentration under real conditions, as well as to assess the durability of the process. This research work was conducted as part of the MaT'Cap (MaTériaux photocatalytiques et Capteurs de la qualité de l'air, i.e., Materials and Sensors for air quality) project funded by the Occitanie Region (South of France) and bringing together three companies—LRVision, Ellona, and PREGA|GA SMART BUILDING—and a university laboratory—Laboratoire Matériaux et Durabilité des Constructions (LMDC)—for a 3-year period. The aim was to assess the air depollution performance of a coating (formulated by LRVision) designed to be applied to the surfaces of existing structures to reduce the concentration of NOx emitted by road traffic, using Ellona® air monitoring stations as an assessment tool. Field experiments were carried out on the scale of canyon streets specifically precast and installed by PREGA|GA SMART BUILDING (off-site concrete

production plant) for the needs of the project, into which artificial pollution (exhaust gases) was injected. NOx concentration was monitored by Ellona® air quality stations, which measured NOx concentrations at various points in the canyons. Coating durability was assessed by comparing the percentage of NO reduction at the reactor scale before and after abrasion cycles, accelerated weathering tests (QUV panel), and immersion in water/drying cycles.

2. Materials and Methods

2.1. Field Experiments for Air Depollution Assessment

2.1.1. Experimental Site

The experimental site, shown in Figure 2a, was located at the PREGA | GA SMART BUILDING plant (Labège, Haute-Garonne, France). Reinforced concrete walls were built by PREGA | GA SMART BUILDING (cement CEM I 52.5 R CE CP2 NF PLN) and assembled to form two canyon streets 3 m high and 10 m long: an untreated control street and a street with 60 m² walls treated with a photocatalytic coating formulated by LRVision SAS (Escalquens, Haute-Garonne, France), with walls within a canyon spaced 3 m apart. These streets were equipped with air quality monitoring stations, referred to as WT1 (Ellona®, Toulouse, Haute-Garonne, France [44]) hereafter (Figure 2b), and with a weather station (Vantage Pro 2 Plus, Davis® Instruments, Météo Concept, Cesson-Sévigné, France). Three WT1 stations were placed in each canyon street, and the weather station was positioned at the top of the middle walls.
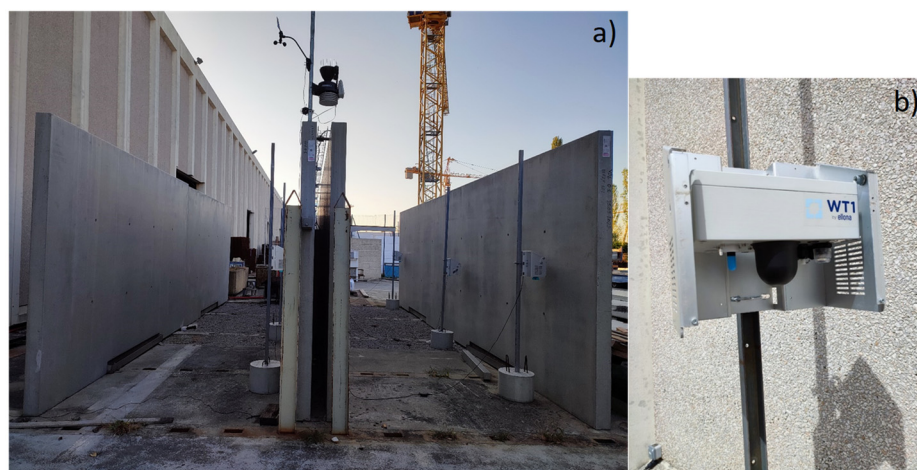
Figure 2. (**a**) Photo of the experimental site: the treated canyon street was on the right, and the untreated (control) canyon street was on the left. Three WT1 air quality stations were installed in each canyon. A weather station was installed at the top of the middle walls. (**b**) WT1 air quality monitoring station.

2.1.2. Coating Application

Before applying the TiO$_2$-based coating, the walls were stripped (laitance and grout film cleaner, vegetable-based formula) to increase the surface porosity of the concrete and optimize coating application. An adjustable-jet sprayer was used for the application (Figure 3a). The canyon walls were then cleaned with water using a high-pressure cleaner (Figure 3b).
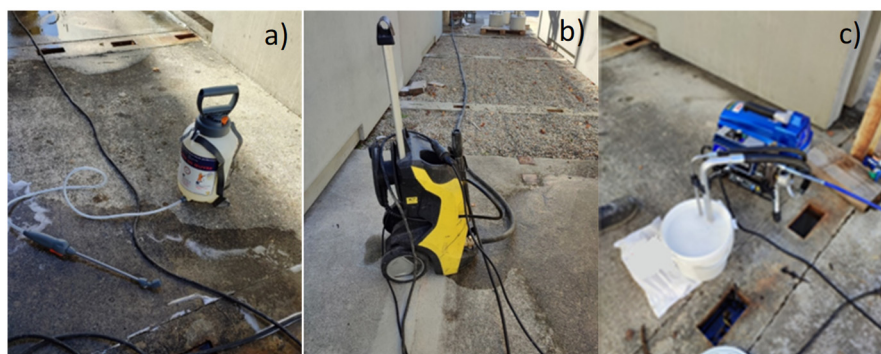
Figure 3. (**a**) Adjustable-jet sprayer used for the application of the laitance and grout film cleaner, (**b**) high-pressure cleaner used to clean canyon walls with water, and (**c**) airless sprayer used to apply the photocatalytic coating to canyon walls.

The rutile-based dispersion (potassium silica as binder, 4 wt.% TiO_2 dry content) was applied using an airless sprayer (Figure 3c). Only one layer was applied to the interior surfaces of the treated canyon (a total of 60 m^2) at a flow rate of 1.0 L/min. The volume of the dispersion was measured before and after the application. A quantity of approximately 4–5 g of TiO_2 per meter square was deposited on the wall surface. The surfaces then dried naturally.

2.1.3. On-Site Air Depollution Experiment

Forced pollution tests were carried out by positioning a diesel vehicle at the entrance to each canyon street to simulate a critical pollution episode in an urban environment, such as heavy road traffic. WT1 air quality monitoring stations were positioned at a height of 1.5 m inside the canyon streets, at a 10 cm (± 0.5 cm) distance from the wall, and at different distances from the source of pollutant emissions (exhaust gases): 1 m, 4 m, and 9 m. The artificial pollution was emitted by the diesel vehicle for 30 min in each canyon street, first in the treated canyon and then in the untreated (control) canyon. Before this, wind measurements were taken for 30 min in each canyon, at 3 different locations—1 m, 4 m, and 9 m (10 min per location)—using an anemometer (WINDVISU, Littoclime SARL, Caen, France), to determine the local wind speed inside each canyon. Weather conditions—temperature, relative humidity, wind speed and direction, and solar irradiance—were obtained from the Davis® Instruments weather station. The frequency of measurement for the WT1 station and anemometer was 10 s, and 15 min for the weather station. A schematic representation of the forced pollution test (diesel vehicle positioned at the entrance to the treated canyon street) is shown in Figure 4.
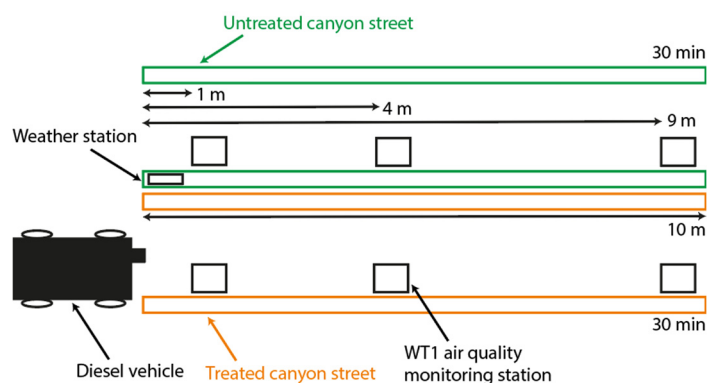
Figure 4. Schematic representation of the experimental site during the forced pollution test in the treated canyon. The experiment lasted 30 min, after which the vehicle was moved to the entrance of the untreated canyon.

2.2. Laboratory Experiments for Durability Assessment

2.2.1. Preparation of Coated Mortar Samples

Normalized mortar (water/ cement ratio of 0.50, 450 g of Portland cement CEM I 52.5, 225 g of water, and 1350 g of 0/2 mm sand) was prepared according to the NF EN 196-1 standard. After mechanical mixing of water, cement, and sand, the fresh mortar was poured into a $30 \times 30 \times 1$ cm^3 steel mold and vibrated for 15 s on a vibrating table. It was left to dry for 7 days before being demolded and sawn into $10 \times 5 \times 1$ cm^3 or $15 \times 5 \times 1$ cm^3 samples using a diamond saw. Prior to the coating application, the mortar surface was ground (120-µm silicon carbide abrasive disk) to smooth the surface and remove the release agent. The photocatalytic coating (the same TiO$_2$-based dispersion used for field application) was then applied to the surface of mortar samples using a fine brush. The quantity deposited on the surface, and therefore the TiO$_2$ dry content, was controlled by weighing the beaker containing the coating with the brush before and after application. A content of 9.5 ± 0.5 g/m^2 of TiO$_2$ was deposited (approximately 0.0475 g for a 50 cm^2 sample) to ensure the accuracy of the weighing. Samples were left to dry at room temperature for 24 h before being tested for air depollution.

2.2.2. Reactor-Scale Air Depollution Experiment

A commercial nitrogen monoxide cylinder (16 ppm of NO balanced in N$_2$, Air Liquide) was used to generate the gaseous pollutant. The flow rate of the NO gas stream was controlled by a mass flow controller. Dry, pollutant-free air was supplied by an air generator (ZAG 7001, Envea SA, Poissy, France). The desired relative humidity (RH) level was achieved by mixing dry air with air passing through a gas washing bottle, the flow rate of each stream being adjusted by mass flow controllers. The NO gas stream and humidified air stream met in a mixing chamber to give a polluted humidified air stream (400 ppb NO, 50% RH), which entered a cylindrical borosilicate glass reactor containing the mortar sample. It was also possible to bypass (bypass route) the reactor to control the level of pollution injected. The NO, NO$_2$, and NOx concentrations were measured by a chemiluminescent analyzer (AC32M, Envea SA, France). This experimental set-up was adapted from ISO 22197-1 [45].

The experimental protocol used to assess the air depollution property of coated mortar samples was previously described by Hot et al. [35,46]. It basically consisted of four main steps: (1) adjusting the desired level of NO pollution (400 ppb) through the bypass route (10 min), (2) injecting polluted air into the reactor containing the sample in the darkness (10 min), (3) switching on the light (30 min), and (4) switching off the light (10 min). A Narva LT-T8 Blacklight blue 18 W 073 fluorescent tube was used to activate the photocatalytic process. The intensity of UV-A light received at the surface of the mortar sample was 5.8 W/m^2. The air depollution property was evaluated by measuring the NO degradation (expressed in percentage) according to Equation (1).

$$\text{NO degradation (\%)} = 100 \times \frac{[\text{NO}]_{\text{initial}} - [\text{NO}]_{\text{final}}}{[\text{NO}]_{\text{initial}}}, \tag{1}$$

where [NO]$_{\text{initial}}$ and [NO]$_{\text{final}}$ were the concentrations in ppb measured by the analyzer at the exit of the reactor before light activation once the steady state was established (step 2), and at the exit of the reactor after light activation and averaged over the last 10 min (step 3), respectively.

2.2.3. Abrasion, Accelerated Weathering, and Immersion/Drying Experiments

The durability of the photocatalytic coating deposited on the mortar surface was evaluated by the changes in the degradation percentage of the NO gaseous pollutant before and after abrasion cycles, accelerated weathering tests, and immersion in water and drying cycles. Equation (2) was used to assess the changes in the NO removal efficiency (ρE). The

higher the ρE value (maximum value of 1), the lower the impact of the durability test on the air depollution capacity of the coating.

$$\rho E = \frac{\text{NO degradation after durabilty test}}{\text{NO degradation before durability test}}, \qquad (2)$$

where NO degradation percentages after and before durability testing were calculated by Equation (1).

Abrasion tests (without water) were carried out according to ASTM D2486 using the Abrasion tester Elcometer® 1720. Mortar samples were exposed to a varying number of cycles—100, 200, or 1000—using a nylon brush and a 3M Scotch Brite® abrasive pad consistent with the ISO 11998 standard. Three different mortar samples were used, each for a specific number of cycles.

Mortar samples subjected to accelerated weathering were obtained after exposure in a QUV panel (model QUV Spray with SOLAR EYE Irradiance Control, Q-LAB) for 252 h (equivalent to 3 months of real-life use), 504 h (equivalent to 6 months of real-life use), and 1008 h (equivalent to 12 months of real-life use) according to NF EN 927-6. The following cycle was applied for one week: (step 1) steam condensation for 24 h (temperature of 45 °C), and (step 2) alternating UV irradiation for 2.5 h (4 fluorescent tubes UV-A 340 nm, 0.89 W/m^2 per tube, temperature of 60 °C)/water spray for 30 min, repeated 48 times. This cycle lasted 168 h. For the 252 h test, the one-week cycle was repeated a second time with step 2 repeated 20 times. For tests lasting 504 h and 1008 h, the one-week cycle was repeated for three weeks and six weeks, respectively. Three different mortar samples were used, each for a specific number of test hours.

Mortar samples were also subjected to immersion/drying cycles according to LRVision's own procedure: 5, 10, 15, and 20 cycles. A cycle consisted of immersion in water for 3 h followed by a drying period of 21 h. Four different mortar samples were used, each for a specific number of cycles. These tests were performed on $15 \times 5 \times 1$ cm^3 mortar samples.

3. Results

3.1. NOx Depollution in Field Conditions

3.1.1. NOx Concentrations

Figure 5 shows the evolution of NO (Figure 5a–c) and NO$_2$ (Figure 5d–f) concentrations measured by the WT1 stations located at different distances in the treated and untreated canyons (TC and UTC) from 9:30 a.m. to 1:30 p.m. (9:30 to 13:30) on a summer's day in June 2023. The forced pollution test in the treated canyon (TC) street was carried out first, from 10:52 to 11:22 a.m., followed by the experiment in the untreated canyon (UTC) street, from noon to 12:30 p.m. (12:00 to 12:30), which explains the offset on the *x*-axis. For a given pollutant (NO or NO$_2$), each graph (a, b, c or d, e, f) corresponds to a distance between the source of pollution and the air quality monitoring station WT1 (1, 4, or 9 m).

The concentrations of NO and NO$_2$ measured during the 30 min forced pollution test carried out in the TC and UTC streets were summed and averaged. The obtained values are summarized in Table 1.
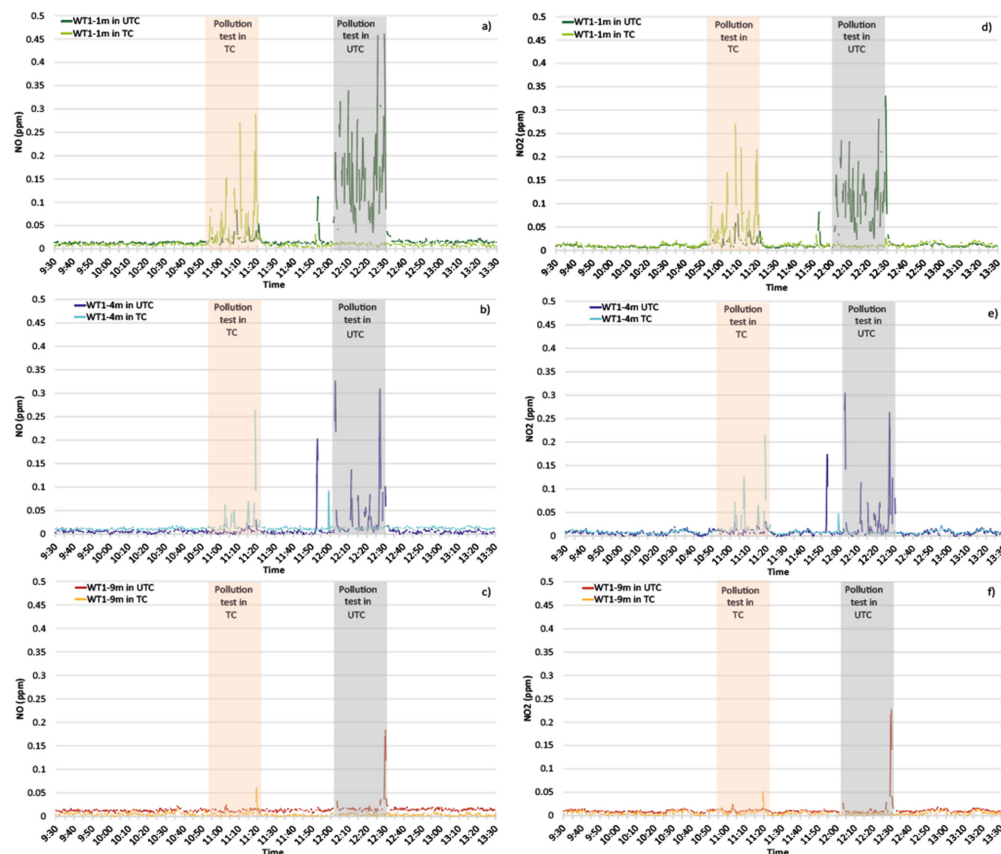
Figure 5. NO and NO$_2$ concentrations obtained during the forced pollution test in the canyon streets—treated canyon (referred to as TC, walls were coated with TiO$_2$-based dispersion) and untreated canyon (control canyon referred to as UTC). Pollution was injected first into the TC street, then into the UTC street. NO and NO$_2$ concentrations were measured by the WT1 stations located at 1 m (**a,d**), 4 m (**b,e**), and 9 m (**c,f**) in the TC and UTC streets.

Table 1. Sum and average of NO and NO$_2$ concentrations obtained during the forced pollution test in the TC and UTC streets. Concentrations were measured by the WT1 stations.

Sum of Concentrations (ppm)					
Canyon	NO (1 m)	NO (4 m)	NO (9 m)	NO$_2$ (1 m)	NO$_2$ (4 m)	NO$_2$ (9 m)
TC	6.6	3.1	0.8	7.0	3.2	1.1
UTC	20.5	5.8	2.6	14.7	5.1	1.9
Average concentrations (ppb)					
Canyon	NO (1 m)	NO (4 m)	NO (9 m)	NO$_2$ (1 m)	NO$_2$ (4 m)	NO$_2$ (9 m)
TC	52.6	24.5	5.7	55.8	24.9	8.6
UTC	159.1	42.6	20.8	113.6	37.7	15.2

3.1.2. Weather Conditions

Forced pollution tests were carried out over a short period of time (less than 2 h) to ensure similar meteorological conditions in the TC and UTC streets. Temperature, relative humidity, wind speed and direction, and solar radiation measured by the weather station positioned at the top of the middle walls are shown in Table 2. Weather conditions were broadly similar, with the exception of the higher solar radiation measured during the test in the UTC street (no photocatalytic effect was expected in this canyon as the walls were not coated with the TiO$_2$-based dispersion) due to the sun path being optimal at noon (which can also explain the higher temperature and lower relative humidity during the test in the UTC). The local average wind speed measured by the anemometer in the canyon

streets (protected from the wind) was less than 1 m/s: 0.75 m/s for the TC and 0.34 m/s for the UTC. Such low wind speed values are associated with stable and calm atmospheric conditions and are not favorable to pollutant dispersion [47,48]. This means that during the forced pollution tests, the wind did not influence the NOx concentration profile.

Table 2. Weather conditions during the forced pollution tests carried out in the TC and UTC streets. These parameters were measured by the weather station located at the top of the middle wall.

Canyon	Temperature (°C)	Relative Humidity (%)	Wind Speed (m/s)	Wind Direction (/)	Solar Irradiance (W/m²)
TC	23.8	67.3	8.0	South–East	487
UTC	24.8	61.7	8.0	South–East	671

3.2. Coating Durability Assessment

For all coated mortar samples, the NO concentration injected into the reactor decreased rapidly due to the activation of the photocatalytic reaction after the UV-A lamp was switched on. The NO concentration returned to its initial value of 400 ppb after the UV-A lamp was switched off. The decrease in NO concentration after light activation was more or less influenced by the type of durability test.

Figure 6 shows the results of abrasion (Figure 6a), QUV (Figure 6b), and immersion/drying (Figure 6c) tests. ρE, as defined by Equation (2), is plotted on the y-axis.
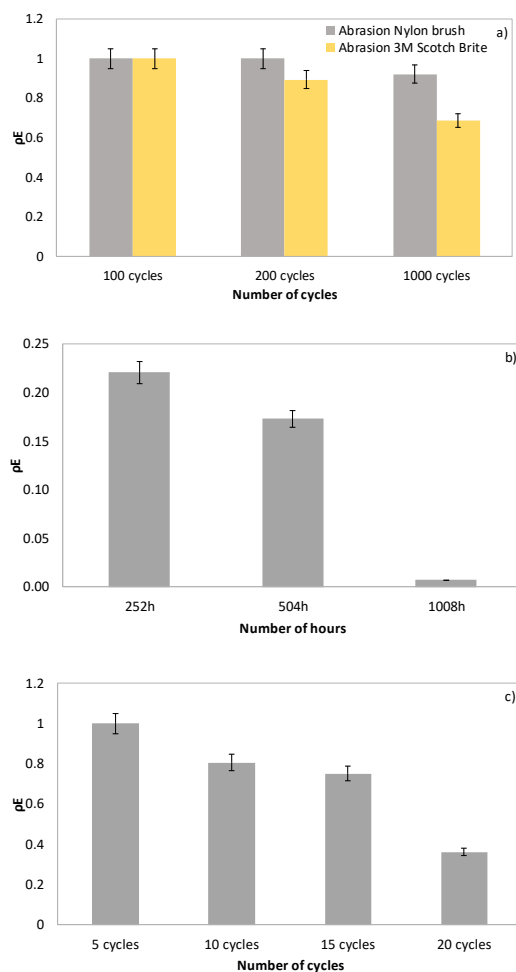

Figure 6. Durability assessment results: (**a**) abrasion test, (**b**) QUV test, and (**c**) water immersion/drying test. The ratio between the percentage of NO degradation after and before the test was calculated and plotted on the y-axis (ρE).

4. Discussion

4.1. NOx Depollution under Field Conditions

Figure 5 shows the raw NOx concentrations obtained during the forced pollution tests. These data revealed that the NO and NO_2 concentration values (concentration peaks) obtained during the pollution injection in the UTC street were higher than those in the TC street. This effect was even more noticeable for the WT1 station located at 1 m, i.e., close to the pollution source. The higher the distance between the pollution source and the measurement point, the lower the NOx concentration (dilution effect) [2]. The decrease in concentrations was clearly highlighted when considering the average NO and NO_2 concentrations obtained during the forced pollution tests: a comparative analysis between the two canyon streets reveals values 2 to 4 times lower for the TC street than for the UTC street (Table 1). As mentioned in the results section, weather conditions were similar during the pollution tests carried out in the TC and UTC streets, so the observed reduction can be attributed to the photocatalytic activity of the coating. A radar representation is suggested in Figure 7 to show the positive impact of the coating on NOx concentration, regardless of the distance from the pollution source. This remediation action will contribute to meeting the EU annual limit of 40 $\mu g/m^3$ and the WHO guideline value of 10 $\mu g/m^3$ for the NO_2 gaseous pollutant.
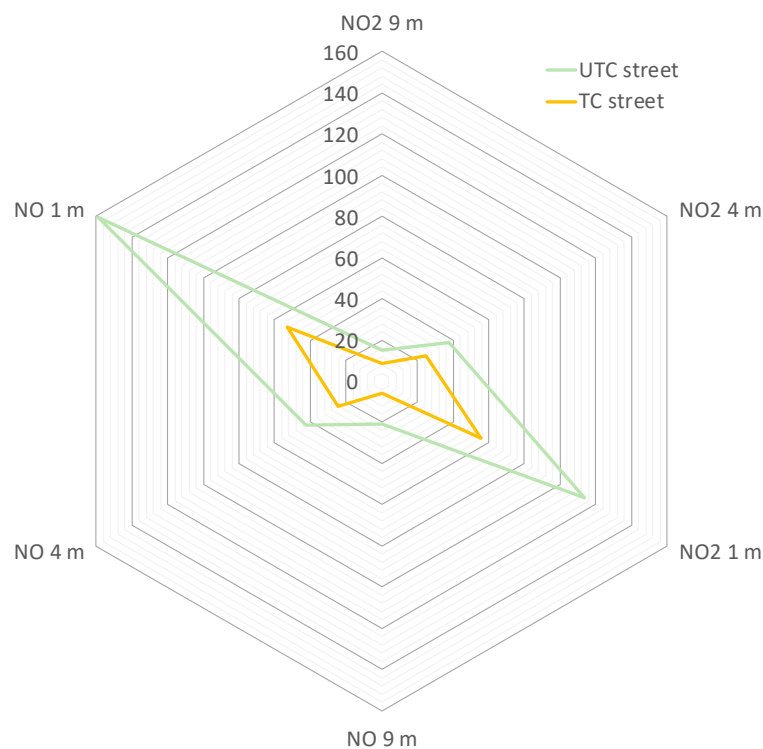
Figure 7. Radar diagram comparing the average NO and NO_2 concentrations (in ppb) obtained during the 30 min forced pollution test at different distances from the pollution source (1, 4, and 9 m), between the UTC street (green) and the TC street (orange).

To go deeper into the analysis, we estimated the probability distribution of NOx concentration during the 30 min forced pollution test in each canyon. The Kernel Density Estimation shown in Equation (3) was used to plot probability density functions for NO and NO_2 concentrations [49]. It gives the density estimate at a point y (a concentration) within a group of points x_i ($i = 1 \dots n$). This means that this function represents the probability

(between 0 and 1) that the concentrations of NO or NO$_2$ will reach a certain value (expressed in ppb). All the computations were carried out using the Python programming language.

$$f(y) = \frac{1}{nh} \sum_{i=1}^{n} K\left(\frac{y - x_i}{h}\right), \tag{3}$$

With $f(y)$ representing the density estimate at point y, x_i a single data point—the i-th point belonging to our dataset (measured NO or NO$_2$ concentrations), n the total number of points in our dataset, h the Kernel smoothing bandwidth as defined by Equation (4) [50], and K the Kernel function equivalent to a Gaussian distribution as defined by Equation (5) [51].

$$h = 1.06 \times \frac{\sigma}{n^{\frac{1}{5}}}, \tag{4}$$

With σ representing the standard deviation of our dataset.

$$K(x) = \frac{1}{\sigma\sqrt{2\pi}} \times e^{-\frac{1}{2}\left(\frac{x-\mu}{\sigma}\right)^2}, \tag{5}$$

With x representing the random variable (here $x = \frac{y-x_i}{h}$), σ the standard deviation of the distribution, and μ the mean of the distribution.

Figure 8 shows the density functions obtained for the NO (Figure 8a–c) and NO$_2$ (Figure 8d–f) concentrations at different distances from the pollution source during the forced pollution test, comparing the UTC street (green) with the TC street (orange). We observed that at distances of 1, 4, and 9 m from the pollution source, measured NO and NO$_2$ concentrations tended to approach the zero value for the TC street. The probability of obtaining lower concentrations was then higher in the canyon street with the photocatalytic coating, meaning that NOx concentration peaks were reduced due to the photocatalytic process. The density function is an interesting statistical approach for assessing the effect of an air remediation action on air quality.
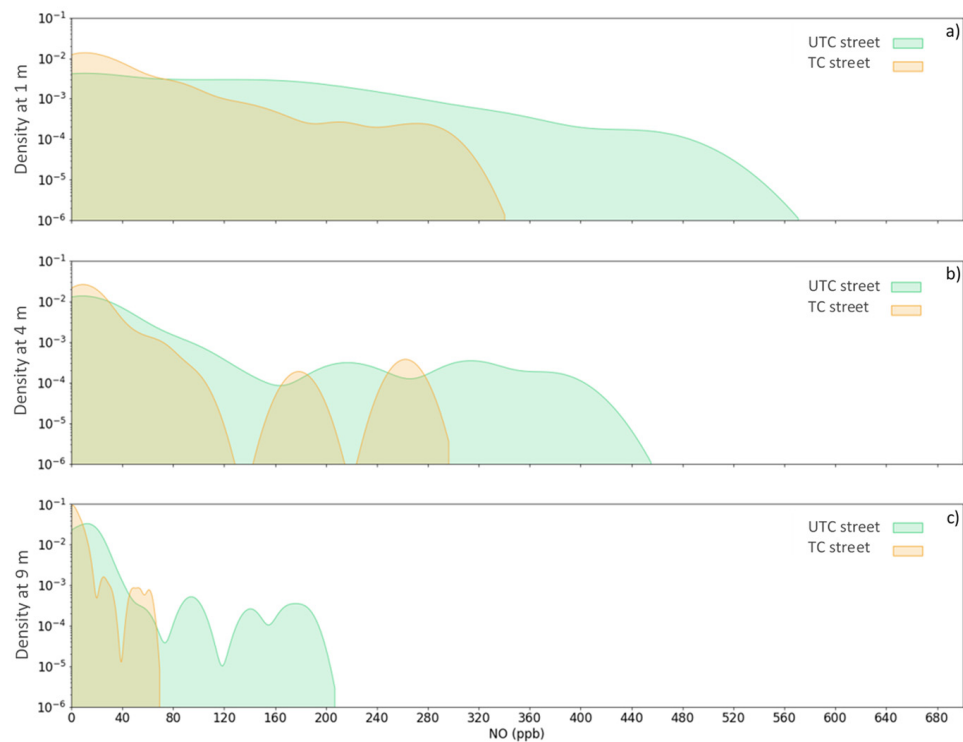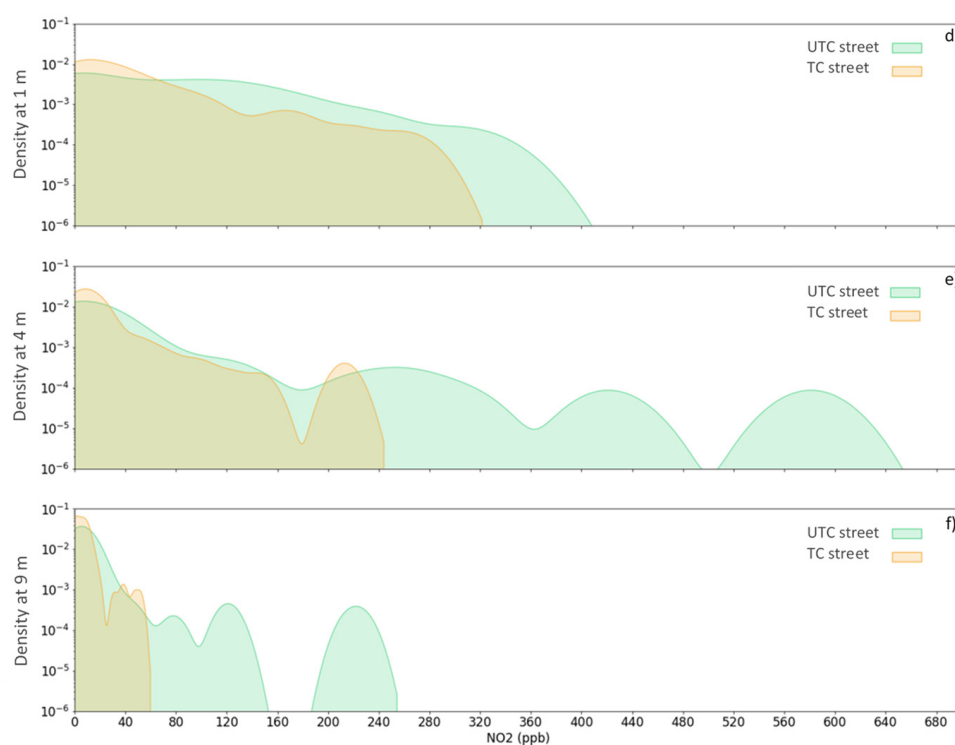

Figure 8. *Cont.*

Figure 8. Probability functions of the NO (**a**–**c**) and NO$_2$ concentrations (**d**–**f**) obtained during the forced pollution test in the UTC and TC streets for different distances from the pollution source (1 m, 4 m, and 9 m). Semi-log scale on the *y*-axis.

At a laboratory reactor scale, air depollution efficiency is assessed by a percentage of degradation (Equation (1)). This percentage can also be calculated in field experiments by comparing the active (with photocatalytic treatment) and control (without photocatalytic treatment) areas over the same period, or before and after the application of a photocatalytic coating/material. In our study, the percentages of NO and NO$_2$ degradation were assessed on the basis of Equation (1) ([NO$_2$] was used instead of [NO] to calculate the percentage of NO$_2$ degradation) and by comparing the average concentration in the UTC street (control area, [NO]$_{initial}$ and [NO$_2$]$_{initial}$) with the average concentration in the TC street (active area, [NO]$_{final}$ and [NO$_2$]$_{final}$). The following degradation percentages were obtained in the TC street: 62% for NO and 46% for NO$_2$. This range of degradation percentages was within that indicated by some previous studies. For example, Maggos et al. reported 36.7 to 83% lower NOx concentrations in a canyon street with TiO$_2$-treated panels compared to the reference canyon street [40]. Cordero et al. studied the photocatalytic efficiency of urban pavements at a pilot scale and obtained removal efficiencies up to 74% and 40% for NO and NO$_2$, respectively [52]. In a demonstration project for photocatalytic pavement reported by Ballari and Brouwers, a 45% reduction in NOx concentration was observed under ideal weather conditions (high radiation and low relative humidity) [53]. Guerrini and Peccati showed an average NO abatement of 51% during a monitoring campaign carried out in Italy comparing a reference area with a road section of an active surface of about 12,000 m^2 [54]. However, literature studies also reported much lower efficiency values, making it difficult to reach a common consensus on the effectiveness of the photocatalytic process under field conditions. This wide variability in air depollution results is notably linked to the influence of environmental conditions (wind, light irradiation, other pollutants, etc.), to a much lower active surface/volume to be depolluted ratio than in a laboratory reactor, to sampling points far from the active surface, and to variable field test methodologies between studies [43].

Moreover, a major problem associated with the evaluation of the efficiency of photocatalytic materials under field conditions comes from the analytical tool used to measure

changes in ambient NOx concentrations in order to map large areas with high spatial and temporal resolution. The cost of a conventional NOx analyzer makes it difficult to implement at different locations during a real-life experiment. The study presented here, therefore, gave an overview of the photocatalytic NOx removal evaluated using low-cost sensors, a technology that should be encouraged in the future to obtain a better representation of air pollution and the efficiency of remediation methods by covering a larger area.

4.2. Laboratory-Scale Durability Assessment

The question of durability was mainly assessed by quantifying changes in the performance of the photocatalytic coating over time, the performance evaluated being either the self-cleaning capacity (water contact angle) or the air depollution property (degradation of a pollutant) [55–57]. Performance loss can be reversible, as in the case of nitrate species or dirt build-up on the surface which can be washed away by rain [58], or irreversible, as in the case of abrasive wear, weathering, or other mechanisms (carbonation of cementitious materials, destruction of polymer binder) [32,59]. The adherence of the photocatalytic coating to the surface is a crucial parameter, especially for asphalt surface applications where abrasive wear is expected in real life due to road traffic. This subject was notably investigated by Wang et al. [60] and Mahy et al. [61], which showed a high dependence of the mechanical resistance on the surface functionalization method. In our work, the coating was applied to walls, meaning that abrasive wear may be limited. The results showed that the nylon brush had no effect on the air depollution capacity of the coating. The test carried out with the 3M Scotch Brite® abrasive pad, which is a much more severe mechanical aggression, led to a 30% reduction ($\rho E = 0.69$) in photocatalytic activity only after 1000 cycles (Figure 6a). The application of photocatalytic coatings to the exterior surface of a building can suffer from weathering caused by prolonged exposure to sunlight, humidity, rain, or manual washing [56,62]. The accelerated weathering test carried out in the QUV panel was designed to simulate the coupling effects of these factors, such as LRVision's own immersion/drying procedure. The results showed a clear negative influence on coating durability from 252 h for the QUV test ($\rho E = 0.22$). This accelerated weathering test reproduces the damage caused by sunlight, rain, and dew that occurs over months or years outdoors with a high degree of severity that may not represent actual conditions. As Baudys et al. pointed out, the relationship between the QUV and outdoor exposure can be misleading because the UV intensity received by the sample in the QUV panel is brighter and shorter, and it does not take into account the fact that natural UV light is extremely variable and can be attenuated due to cloud cover, shading, and changes in the course of the solar spectrum changes throughout the year [63]. In particular, they estimated that, under the specific UV irradiation conditions set in the QUV chamber and for the city of Prague, QUV lamps are 12 times brighter than solar UV. The immersion/drying test gave rise to less severe weather conditions (notably the absence of UV irradiation), with a clear reduction in air depollution capacity observed from the last number of cycles tested, i.e., 20 cycles ($\rho E = 0.36$).

5. Conclusions

The development of photocatalytic coatings based on the semiconductor TiO_2 is a research field where many challenges remain in producing a material with long-lasting high performance at an industrial scale. Durability is essential for assessing the viability of photocatalytic surfaces but receives less attention in the literature. The same applies to the evaluation of their efficiency under real-life conditions. The aim of this article was to present further results on these two aspects of the photocatalytic process.

The air depollution property of a TiO_2-based photocatalytic coating was evaluated under real-life conditions at the scale of a canyon street. A diesel vehicle was used to artificially inject pollution into a wall-coated canyon street and a control (untreated) canyon street. NOx concentration was measured by air quality stations providing multiple sampling points in the canyon streets at different distances from the pollution source. The raw

data were used for statistical analysis. The results showed that the canyon street whose walls were coated had lower NO and NO_2 concentrations than the control canyon street, this effect being more pronounced in the vicinity of the pollution source (at 1 m). NOx concentration also fell naturally with distance from the source due to the dilution effect. This means that such a remediation process could help to meet the WHO NO_2 guidelines and improve air quality, particularly near high-traffic areas.

The resistance of the photocatalytic coating to mechanical abrasion and accelerated weathering was then tested on the scale of a laboratory reactor. The coating tested exhibited good mechanical durability, although a 30% reduction was observed under the most severe conditions, i.e., after 1000 abrasion cycles with a 3M Scotch Brite® abrasive pad. The air depollution capacity of the coating was reduced by 65% for the highest number of cycles during the immersion/drying test. The most significant reduction in air depollution efficiency was observed during the QUV test, where simulated accelerated weathering conditions can be far from real outdoor exposure.

In future studies, it will be absolutely necessary to further investigate the real-scale application and durability of the photocatalytic process, and to use automatic monitoring systems such as sensors, in order to optimize data collection over a longer period of time and a wider geographical area.

Data Availability Statement: The data presented in this study are available upon request from the corresponding author.

Conflicts of Interest: This research work was carried out as part of a collaborative project. The authors declare no conflicts of interest. Author Erick Ringot is a former co-manager of the company LRVision. The remaining authors declare that the research was conducted in the absence of any commercial or financial relationships that could be construed as a potential conflict of interest.

References

1. World Health Organization. 9 out of 10 People Worldwide Breathe Polluted Air. Available online: http://www.emro.who.int/media/news/9-out-of-10-people-worldwide-breathe-polluted-air.html (accessed on 30 May 2024).
2. Pearson, R.L.; Wachtel, H.; Ebi, K.L. Distance-Weighted Traffic Density in Proximity to a Home Is a Risk Factor for Leukemia and Other Childhood Cancers. *J. Air Waste Manag. Assoc.* **2000**, *50*, 175–180. [CrossRef]
3. Janssen, N.A.H.; Brunekreef, B.; van Vliet, P.; Aarts, F.; Meliefste, K.; Harssema, H.; Fischer, P. The Relationship between Air Pollution from Heavy Traffic and Allergic Sensitization, Bronchial Hyperresponsiveness, and Respiratory Symptoms in Dutch Schoolchildren. *Environ. Health Perspect.* **2003**, *111*, 1512–1518. [CrossRef] [PubMed]
4. McConnell, R.; Berhane, K.; Yao, L.; Jerrett, M.; Lurmann, F.; Gilliland, F.; Künzli, N.; Gauderman, J.; Avol, E.; Thomas, D.; et al. Traffic, Susceptibility, and Childhood Asthma. *Environ. Health Perspect.* **2006**, *114*, 766–772. [CrossRef] [PubMed]

5. Harm to Human Health from Air Pollution in Europe: Burden of Disease 2023—European Environment Agency. Available online: https://www.eea.europa.eu/publications/harm-to-human-health-from-air-pollution (accessed on 30 April 2024).
6. Bai, L.; Shin, S.; Burnett, R.T.; Kwong, J.C.; Hystad, P.; van Donkelaar, A.; Goldberg, M.S.; Lavigne, E.; Weichenthal, S.; Martin, R.V.; et al. Exposure to Ambient Air Pollution and the Incidence of Lung Cancer and Breast Cancer in the Ontario Population Health and Environment Cohort. *Int. J. Cancer* **2020**, *146*, 2450–2459. [CrossRef]
7. Liang, H.; Zhou, X.; Zhu, Y.; Li, D.; Jing, D.; Su, X.; Pan, P.; Liu, H.; Zhang, Y. Association of Outdoor Air Pollution, Lifestyle, Genetic Factors with the Risk of Lung Cancer: A Prospective Cohort Study. *Environ. Res.* **2023**, *218*, 114996. [CrossRef]
8. Air Pollution in Europe: 2023 Reporting Status under the National Emission Reduction Commitments Directive—European Environment Agency. Available online: https://www.eea.europa.eu/publications/national-emission-reduction-commitments-directive-2023 (accessed on 30 April 2024).
9. Pandey, J.S.; Kumar, R.; Devotta, S. Health Risks of NO_2, SPM and SO_2 in Delhi (India). *Atmos. Environ.* **2005**, *39*, 6868–6874. [CrossRef]
10. Ryan, R.G.; Rhodes, S.; Tully, M.; Schofield, R. Surface Ozone Exceedances in Melbourne, Australia Are Shown to Be under NOx Control, as Demonstrated Using Formaldehyde: NO_2 and Glyoxal:Formaldehyde Ratios. *Sci. Total Environ.* **2020**, *749*, 141460. [CrossRef]
11. Stavrakou, T.; Müller, J.-F.; Bauwens, M.; Boersma, K.F.; van Geffen, J. Satellite Evidence for Changes in the NO_2 Weekly Cycle over Large Cities. *Sci. Rep.* **2020**, *10*, 10066. [CrossRef] [PubMed]
12. Vohra, K.; Marais, E.A.; Bloss, W.J.; Schwartz, J.; Mickley, L.J.; Van Damme, M.; Clarisse, L.; Coheur, P.-F. Rapid Rise in Premature Mortality Due to Anthropogenic Air Pollution in Fast-Growing Tropical Cities from 2005 to 2018. *Sci. Adv.* **2022**, *8*, eabm4435. [CrossRef]
13. Sayegh, A.; Tate, J.E.; Ropkins, K. Understanding How Roadside Concentrations of NOx Are Influenced by the Background Levels, Traffic Density, and Meteorological Conditions Using Boosted Regression Trees. *Atmos. Environ.* **2016**, *127*, 163–175. [CrossRef]
14. Ehrnsperger, L.; Klemm, O. Air Pollution in an Urban Street Canyon: Novel Insights from Highly Resolved Traffic Information and Meteorology. *Atmos. Environ. X* **2022**, *13*, 100151. [CrossRef]
15. Ghazali, N.A.; Ramli, N.A.; Yahaya, A.S.; Yusof, N.F.F.M.D.; Sansuddin, N.; Al Madhoun, W.A. Transformation of Nitrogen Dioxide into Ozone and Prediction of Ozone Concentrations Using Multiple Linear Regression Techniques. *Environ. Monit Assess* **2010**, *165*, 475–489. [CrossRef] [PubMed]
16. Han, S.; Bian, H.; Feng, Y.; Liu, A.; Li, X.; Zeng, F.; Zhang, X. Analysis of the Relationship between O_3, NO and NO_2 in Tianjin, China. *Aerosol. Air Qual. Res.* **2011**, *11*, 128–139. [CrossRef]
17. Shukla, J.B.; Sundar, S.; Sharma, S.D.; Naresh, R. Modeling and Analysis of the Acid Rain Formation Due to Precipitation and Its Effect on Plant Species. *Nat. Resour. Model.* **2013**, *26*, 53–65. [CrossRef]
18. World Health Organization. What Are the WHO Air Quality Guidelines? Available online: https://www.who.int/news-room/feature-stories/detail/what-are-the-who-air-quality-guidelines (accessed on 30 May 2024).
19. Managing Air Quality in Europe—European Environment Agency. Available online: https://www.eea.europa.eu/publications/managing-air-quality-in-europe/managing-air-quality-in-europe (accessed on 30 April 2024).
20. Europe's Air Quality Status 2023—European Environment Agency. Available online: https://www.eea.europa.eu/publications/europes-air-quality-status-2023/europes-air-quality-status2023/#fn1 (accessed on 30 April 2024).
21. Shelef, M.; Otto, K.; Gandhi, H. The Oxidation of CO by O_2 and by NO on Supported Chromium Oxide and Other Metal Oxide Catalysts. *J. Catal.* **1968**, *12*, 361–375. [CrossRef]
22. Solymosi, F.; Kiss, J. Adsorption and Reduction of NO on Tin(IV) Oxide Catalysts. *J. Catal.* **1976**, *41*, 202–211. [CrossRef]
23. Solymosi, F.; Kiss, J. Adsorption and Reduction of NO on Tin(IV) Oxide Doped with Chromium(III) Oxide. *J. Catal.* **1978**, *54*, 42–51. [CrossRef]
24. Lim, T.H.; Jeong, S.M.; Kim, S.D.; Gyenis, J. Photocatalytic Decomposition of NO by TiO_2 Particles. *J. Photochem. Photobiol. A Chem.* **2000**, *134*, 209–217. [CrossRef]
25. Ângelo, J.; Andrade, L.; Madeira, L.M.; Mendes, A. An Overview of Photocatalysis Phenomena Applied to NOx Abatement. *J. Environ. Manag.* **2013**, *129*, 522–539. [CrossRef]
26. Nema, A.; Kaul, D.S.; Mukherjee, K.; Jeyaraman, J.D. Photo-Active Catalysts in Building and Construction Materials for Air Pollution Treatment: A Bibliometric Analysis. *Mater. Today Proc.* **2022**, *62*, 7297–7301. [CrossRef]
27. Recent Progress and Current Status of Photocatalytic NO Removal|IntechOpen. Available online: https://www.intechopen.com/chapters/88123 (accessed on 30 July 2024).
28. Castelló Lux, K.; Hot, J.; Fau, P.; Bertron, A.; Kahn, M.; Ringot, E.; Fajerwerg, K. Nano-gold decorated ZnO: An alternative photocatalyst promising for NOx degradation. *Chem. Eng. Sci.* **2023**, *267*, 118377. [CrossRef]
29. Henderson, M.A. A Surface Science Perspective on TiO_2 Photocatalysis. *Surf. Sci. Rep.* **2011**, *66*, 185–297. [CrossRef]
30. Fujishima, A.; Rao, T.N.; Tryk, D.A. Titanium Dioxide Photocatalysis. *J. Photochem. Photobiol. C Photochem. Rev.* **2000**, *1*, 1–21. [CrossRef]
31. Fujishima, A.; Zhang, X.; Tryk, D.A. TiO_2 Photocatalysis and Related Surface Phenomena. *Surf. Sci. Rep.* **2008**, *63*, 515–582. [CrossRef]

32. Kaja, A.M.; Brouwers, H.J.H.; Yu, Q.L. NOx Degradation by Photocatalytic Mortars: The Underlying Role of the CH and C-S-H Carbonation. *Cem. Concr. Res.* **2019**, *125*, 105805. [CrossRef]

33. Chen, X.; Qiao, L.; Zhao, R.; Wu, J.; Gao, J.; Li, L.; Chen, J.; Wang, W.; Galloni, M.G.; Scesa, F.M.; et al. Recent Advances in Photocatalysis on Cement-Based Materials. *J. Environ. Chem. Eng.* **2023**, *11*, 109416. [CrossRef]

34. Zouzelka, R.; Rathousky, J. Photocatalytic Abatement of NOx Pollutants in the Air Using Commercial Functional Coating with Porous Morphology. *Appl. Catal. B Environ.* **2017**, *217*, 466–476. [CrossRef]

35. Hot, J.; Topalov, J.; Ringot, E.; Bertron, A. Investigation on Parameters Affecting the Effectiveness of Photocatalytic Functional Coatings to Degrade NO: TiO_2 Amount on Surface, Illumination, and Substrate Roughness. *Int. J. Photoenergy* **2017**, *2017*, e6241615. [CrossRef]

36. Hot, J.; Martinez, T.; Wayser, B.; Ringot, E.; Bertron, A. Photocatalytic Degradation of NO/NO_2 Gas Injected into a 10-M3 Experimental Chamber. *Environ. Sci. Pollut. Res.* **2017**, *24*, 12562–12570. [CrossRef]

37. Hot, J.; Bradley, P.; Cooper, J.; Wayser, B.; Ringot, E. In Situ Investigation of NO_x Photocatalytic Degradation: Case Study in an Open Space Office in Manchester, UK. *Health Environ.* **2020**, *1*, 28–37. [CrossRef]

38. Xie, X.; Hao, C.; Huang, Y.; Huang, Z. Influence of TiO_2-Based Photocatalytic Coating Road on Traffic-Related NOx Pollutants in Urban Street Canyon by CFD Modeling. *Sci. Total Environ.* **2020**, *724*, 138059. [CrossRef] [PubMed]

39. Nosek, Š.; Ducháček, T.; Magyar, P.; Procházka, J. The Role of Flow Structures in the Effective Removal of NOx Pollutants by a TiO_2-Based Coating in a Street Canyon. *J. Environ. Chem. Eng.* **2023**, *11*, 109758. [CrossRef]

40. Maggos, T.; Plassais, A.; Bartzis, J.G.; Vasilakos, C.; Moussiopoulos, N.; Bonafous, L. Photocatalytic Degradation of NOx in a Pilot Street Canyon Configuration Using TiO_2-Mortar Panels. *Environ. Monit Assess* **2008**, *136*, 35–44. [CrossRef] [PubMed]

41. Folli, A.; Strøm, M.; Madsen, T.P.; Henriksen, T.; Lang, J.; Emenius, J.; Klevebrant, T.; Nilsson, Å. Field Study of Air Purifying Paving Elements Containing TiO_2. *Atmos. Environ.* **2015**, *107*, 44–51. [CrossRef]

42. Brattich, E.; Barbano, F.; Pulvirenti, B.; Pilla, F.; Bacchetti, M.; Di Sabatino, S. The Effect of Photocatalytic Coatings on NOx Concentrations in Real-World Street Canyons. *Build. Environ.* **2021**, *205*, 108312. [CrossRef]

43. Russell, H.S.; Frederickson, L.B.; Hertel, O.; Ellermann, T.; Jensen, S.S. A Review of Photocatalytic Materials for Urban NOx Remediation. *Catalysts* **2021**, *11*, 675. [CrossRef]

44. Ellona WT1 Outdoor Offer. Available online: https://www.ellona.io/outdoor-offer/ (accessed on 7 June 2024).

45. *ISO 22197-1:2016*; Fine Ceramics (Advanced Ceramics, Advanced Technical Ceramics)—Test Method for Air-Purification Performance of Semiconducting Photocatalytic Materials—Part 1: Removal of Nitric Oxide. ISO: Geneva, Switzerland, 2016.

46. Hot, J.; Ringot, E.; Koufi, L.; Bertron, A. Modelling of NO Photocatalytic Degradation in an Experimental Chamber. *Chem. Eng. J.* **2020**, *408*, 127298. [CrossRef]

47. Coppalle, A.; Delmas, V.; Bobbia, M. Variability of Nox and NO_2 Concentrations Observed at Pedestrian Level in the City Centre of a Medium Sized Urban Area. *Atmos. Environ.* **2001**, *35*, 5361–5369. [CrossRef]

48. Grundström, M.; Hak, C.; Chen, D.; Hallquist, M.; Pleijel, H. Variation and Co-Variation of PM_{10}, Particle Number Concentration, NOx and NO_2 in the Urban Air—Relationships with Wind Speed, Vertical Temperature Gradient and Weather Type. *Atmos. Environ.* **2015**, *120*, 317–327. [CrossRef]

49. Liu, H.; Duan, Z.; Chen, C. A Hybrid Multi-Resolution Multi-Objective Ensemble Model and Its Application for Forecasting of Daily $PM_{2.5}$ Concentrations. *Inf. Sci.* **2020**, *516*, 266–292. [CrossRef]

50. Harpole, J.K.; Woods, C.M.; Rodebaugh, T.L.; Levinson, C.A.; Lenze, E.J. How Bandwidth Selection Algorithms Impact Exploratory Data Analysis Using Kernel Density Estimation. *Psychol. Methods* **2014**, *19*, 428–443. [CrossRef] [PubMed]

51. Oh, Y.; Lyu, P.; Ko, S.; Min, J.; Song, J. Enhancing Broiler Weight Estimation through Gaussian Kernel Density Estimation Modeling. *Agriculture* **2024**, *14*, 809. [CrossRef]

52. Cordero, J.M.; Hingorani, R.; Jimenez-Relinque, E.; Grande, M.; Borge, R.; Narros, A.; Castellote, M. NOx Removal Efficiency of Urban Photocatalytic Pavements at Pilot Scale. *Sci. Total Environ.* **2020**, *719*, 137459. [CrossRef] [PubMed]

53. Ballari, M.M.; Brouwers, H.J.H. Full Scale Demonstration of Air-Purifying Pavement. *J. Hazard. Mater.* **2013**, *254–255*, 406–414. [CrossRef] [PubMed]

54. Guerrini, G.L.; Peccati, E. Photocatalytic Cementitious Roads for Depollution. In Proceedings of the International RILEM Symposium on Photocatalysis, Environment and Construction Materials, Florence, Italy, 8–9 October 2007.

55. Yang, L.; Hakki, A.; Wang, F.; Macphee, D.E. Photocatalyst Efficiencies in Concrete Technology: The Effect of Photocatalyst Placement. *Appl. Catal. B Environ.* **2018**, *222*, 200–208. [CrossRef]

56. Feng, J.; Feng, Q.; Xin, J.; Liang, Q.; Li, X.; Chen, K.; Teng, J.; Wang, S.; Feng, L.; Liu, J. Fabrication of Durable Self-Cleaning Photocatalytic Coating with Long-Term Effective Natural Light Photocatalytic Degradation Performance. *Chemosphere* **2023**, *336*, 139316. [CrossRef] [PubMed]

57. Liu, G.; Zhao, T.; Fei, H.; Li, F.; Guo, W.; Yao, Z.; Feng, Z. A Review of Various Self-Cleaning Surfaces, Durability and Functional Applications on Building Exteriors. *Constr. Build. Mater.* **2023**, *409*, 134084. [CrossRef]

58. Chen, M.; Chu, J.-W. NOx Photocatalytic Degradation on Active Concrete Road Surface—From Experiment to Real-Scale Application. *J. Clean. Prod.* **2011**, *19*, 1266–1272. [CrossRef]

59. de Melo, J.V.S.; Trichês, G.; Gleize, P.J.P.; Villena, J. Development and Evaluation of the Efficiency of Photocatalytic Pavement Blocks in the Laboratory and after One Year in the Field. *Constr. Build. Mater.* **2012**, *37*, 310–319. [CrossRef]

60. Wang, D.; Leng, Z.; Yu, H.; Hüben, M.; Kollmann, J.; Oeser, M. Durability of Epoxy-Bonded TiO$_2$-Modified Aggregate as a Photocatalytic Coating Layer for Asphalt Pavement under Vehicle Tire Polishing. *Wear* **2017**, *382–383*, 1–7. [CrossRef]
61. Mahy, J.G.; Paez, C.A.; Hollevoet, J.; Courard, L.; Boonen, E.; Lambert, S.D. Durable Photocatalytic Thin Coatings for Road Applications. *Constr. Build. Mater.* **2019**, *215*, 422–434. [CrossRef]
62. Wu, Y.; Dong, L.; Shu, X.; Yang, Y.; She, W.; Ran, Q. A Review on Recent Advances in the Fabrication and Evaluation of Superhydrophobic Concrete. *Compos. Part B Eng.* **2022**, *237*, 109867. [CrossRef]
63. Baudys, M.; Krýsa, J.; Mills, A. Smart Inks as Photocatalytic Activity Indicators of Self-Cleaning Paints. *Catal. Today* **2017**, *280*, 8–13. [CrossRef]